Phase decomposition and its applications

SATINDER CHOPRA

SAMIGEO, CALGARY, SATINDER.CHOPRA@SAMIGEO.COM

RITESH KUMAR SHARMA

SAMIGEO, CALGARY

JOHN CASTAGNA

THE UNIVERSITY OF HOUSTON

KENNETH BREDESEN

GEOLOGICAL SURVEY OF DENMARK AND GREENLAND (GEUS), COPENHAGEN

Abstract

We discuss the recently introduced phase decomposition analysis, which entails amplitude variation with time as a function of the seismic reflection phase. Assuming a zero-phase wavelet embedded in the seismic data, while flat spots or unresolved water contacts may be seen on the zero-phase component, in seismically thin layers, impedance changes will show up on phase components that are 90° out of phase with the wavelet. Thus, bright spots caused by thin hydrocarbon reservoirs are associated with low impedance and show up on the phase component that is −90° out of phase with the seismic wavelet. In all cases the interpretation of bright spots is found to be convenient, and easier, with the use of the −90° seismic phase component. In this study, application of phase decomposition are first demonstrated through synthetic data examples, followed by a real seismic data example. In particular, the case study from a gas storage reservoir in Denmark shows that phase decomposition can aid interpretation and reservoir monitoring efforts.

Introduction

Phase decomposition is a novel technique that decomposes a composite seismic signal into different phase components, which can improve reservoir characterization. The technique is particularly useful in those areas where thin-bed interference causes the phase of the input seismic response to differ from the phase of the embedded wavelet in the data. For a zero-phase wavelet in the data and thin low-impedance layers below tuning thickness, the −90° phase component stands out anomalously. A corresponding high-impedance thin layer exhibits a similar +90° phase component response. Furthermore, for thin layers, a change in impedance is best seen on these plus or minus 90° components. By generating a synthetic response with use of well data and a zero-phase wavelet, such observations for thin reservoir layers can be understood with confidence and correlated with real seismic data. Phase decomposition can

help immensely in direct interpretation of seismic data in terms of reservoir and non-reservoir zones, amongst other applications.

Another important aspect is that the seismic waveform is amplitude, phase, and frequency dependent. Phase decomposition does not use well data for the generation of phase components, but the synthetic traces generated from well data can be used to establish the relationships between amplitude/phase/frequency for a given problem. In this context, the application of spectral decomposition to a synthetic trace would produce a frequency gather and provide the required frequency dependent behavior. Likewise, the application of phase decomposition to the generated synthetic gather will provide a set of phase component gathers. Thus, between the spectral and phase decomposition applications, the desired amplitude/phase/frequency information can be found.

We begin this article with a brief description of some of the spectral decomposition techniques available in different commercial software packages, and then showcase their application to a seismic dataset under study. We take the discussion forward from there to the description of phase decomposition and its applications.

Phase decomposition, phase gathers, and generation of individual phase components at 0°, 180°, −90° and +90°, appear to be most useful for interpretation of rock and fluid properties. Defining the odd phase component as the sum of +90° and −90° phase components, we demonstrate that the odd phase component helps delineate a gas reservoir better in accordance with the status of the available wells over the reservoir.

Spectral decomposition

Spectral decomposition is an effective way of analyzing the seismic response of stratigraphic geologic features. It is carried out by transforming the seismic data from the time domain into the frequency domain. This can be done simply by using the short time window discrete Fourier transform (STFT; Partyka et al.,1999), but there are other methods that can be used for the purpose, namely the continuous wavelet transform (CWT; Chakraborty and Okaya, 1995; Sinha et al., 2005), S-transform (Stockwell et al., 1996), matching pursuit (Mallat and Zhang, 1993), constrained least-squares spectral analysis (CLSSA; Puryear et al., 2012), and the optimal Gaussian spectral analysis (OGSA; Lindner et al.,2014). Some of these methods have been used extensively in reservoir characterization exercises, and the literature is replete with different case studies. Using any of the above spectral decomposition methods, the input seismic data volume is decomposed into amplitude and phase volumes at discrete frequencies within the bandwidth of the data, which can then be displayed and interpreted. Alternatively, the output data can be sorted into time-frequency displays, also called gathers, for amplitude and phase.

In this article we begin with a comparison of the frequency gathers for amplitude and phase generated with the application of the following methods.

- STFT: The discrete Fourier transform uses a time window for its computation, and this choice has a bearing on the resolution of the output data.
- CWT: The continuous wavelet transform depends on the choice of the mother wavelet, and usually yields higher spectral resolution but reduced temporal resolution at low frequencies.
- CLSSA: Uses an inversion-based algorithm for computing the spectral decomposition of seismic data and is performed by the inversion of a basis of truncated sinusoidal kernels in a short time window. The method results in a time-frequency analysis with excellent time and frequency resolution and with a time-frequency product superior to the STFT and the CWT.
- OGSA: This process uses a series of frequency domain Gaussian functions to decompose the spectrum of the data, which is carried out in the frequency domain. The result is the superposition of Gaussian functions that are seen to better correlate or match the spectrum of the seismic.

In Figure 1 we show the spectral amplitude gathers for a particular seismic trace shown to the left. We see that these amplitude gathers generated with the application of some of the methods mentioned above are comparable, though differing in temporal and frequency resolution. However, we also notice that the equivalent phase information depicted on such displays or on 'phase' gathers generated by the same set of methods and displayed in Figure 2 appear to be complicated in terms of their interpretative value.

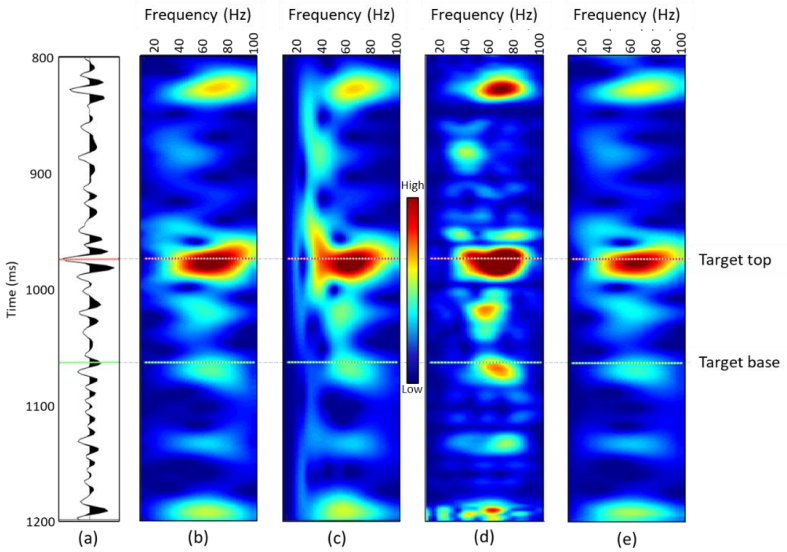

Figure 1: Spectral decomposition on a seismic trace in (a) with the generated amplitude frequency gathers using the (b) STFT (40 ms window), (c) CWT, (d) CLSSA (40 ms window), and (e) OGSA methods. The two horizontal dotted lines in red and green are the levels of the two markers shown for reference.

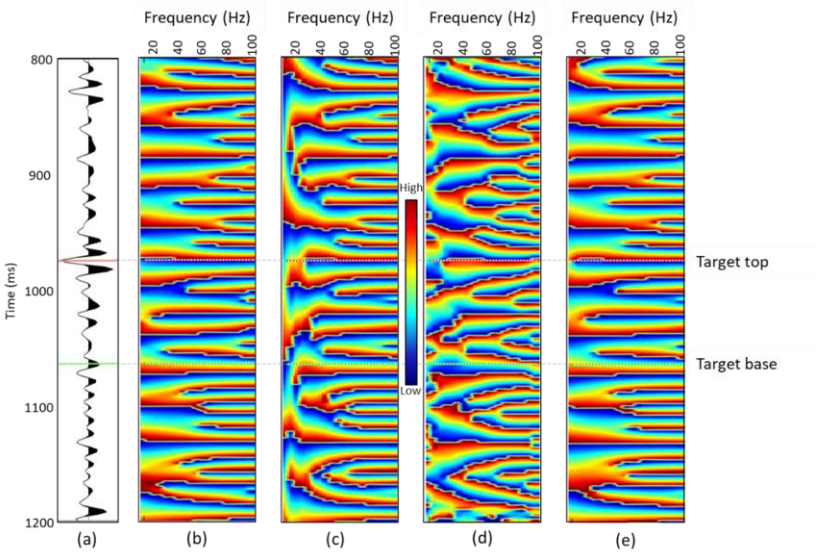

Figure 2: Spectral decomposition on a seismic trace in (a) with the generated phase frequency gathers using the (b) STFT (40 ms window), (c) CWT, (d) CLSSA (40 ms window), and (e) OGSA methods. The two horizontal dotted lines in red and green are the levels of the two markers shown for reference.

Phase decomposition

Castagna et al. (2016) introduced an alternative approach for understanding the phase of the seismic trace by distributing the amplitude and phase spectra such that the amplitude can be expressed as a function of phase as well as frequency. In general, as stated above, the application of spectral decomposition on a seismic trace produces a time-frequency analysis, which when integrated over the data frequency range will recover the original trace. In this analysis it is possible to introduce phase as a third dimension such that a time-phase analysis, or a phase gather, can be generated, which essentially represents the amplitude as a function of time for individual phase components of the seismic trace. When integrated over the complete phase range, the original seismic trace can be reconstructed.

For gaining an insight into this process, a synthetic seismic trace generated with the use of a few Ricker wavelets is shown in solid blue to the right in Figure 3. To the left is the phase gather generated for the blue synthetic seismic trace, which exhibits a good correlation with the phase information indicated on the original seismic trace. On summing this time phase panel over phase, the original seismic trace can be reconstructed and is shown as red dots overlaid on the solid blue original trace. An interesting observation that can be made here is that any phase component (or sum of phase components) of the seismic trace as seen on the phase panel can be extracted and reconstructed. A significant implication of this observation is that phase decomposition can be used as a powerful tool that may be put to use for accentuating or suppressing seismic events with specific spectral characteristics. This process is referred to as ***phase filtering***.

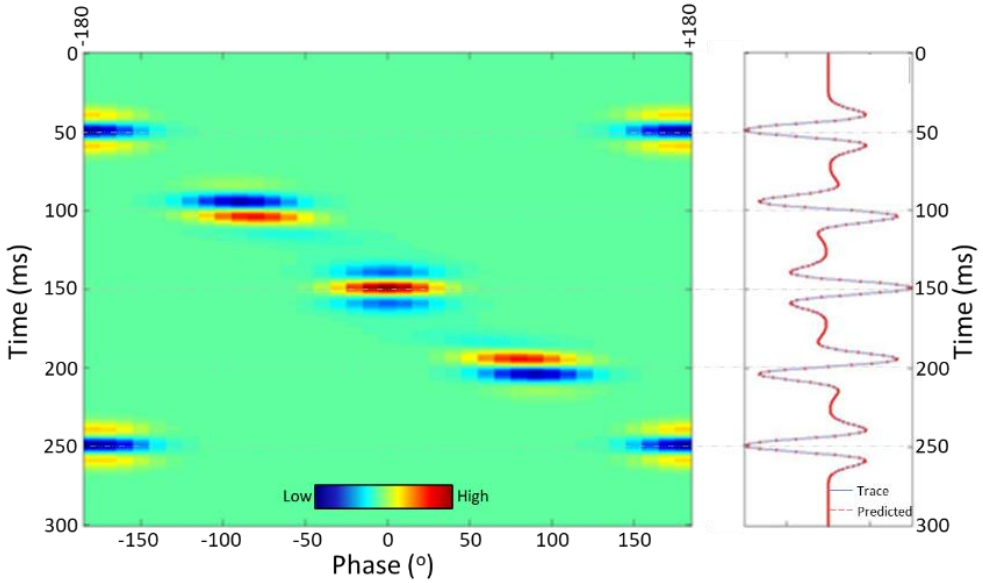

Figure 3: Illustration of seismic phase decomposition. A synthetic seismic trace (solid blue) is shown to the right and the generated time-phase panel or phase gather for it is shown to the left. When the time-phase panel is summed over phase, the original trace is reconstructed and is shown overlaid as dashed red on the solid blue trace to the

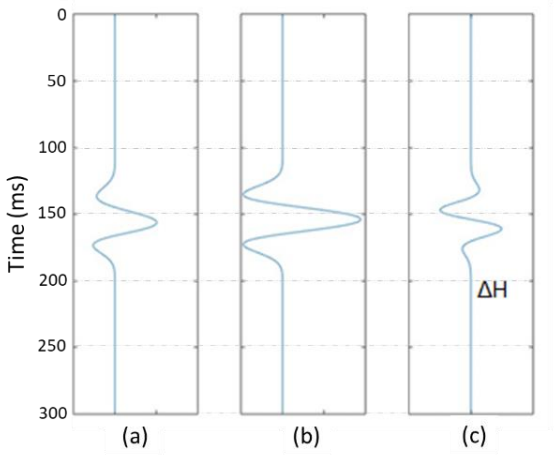

right.

Figure 4: Synthetic waveforms for a seismically thin layer using a zero-phase wavelet resulting in a “dim spot” when gas is added (a). Both brine (b) and gas-filled cases (a) have impedance intermediate between the overlying and underlying impedances, yielding a zero-phase waveform for both cases. Notice the hydrocarbon effect, ΔH, which is the gas response minus the brine response, has a −90° phase rotation with respect to the nearly zero-phase wavelet (c).

As mentioned in the introduction, a unique difference in response between thin hydrocarbon-bearing reservoirs exhibiting low impedance and the same reservoir rock with 100% water saturation and higher impedance is found to occur on the phase component that is out of phase with the embedded zero-phase seismic wavelet. We demonstrate this in Figure 4 which shows a

zero-phase response representing a brine-filled thin layer with impedance intermediate between overlying and underlying half-spaces (middle) as well as the waveform associated with a similar layer bearing gas, also with intermediate impedance (left panel). For seismically thin layers, the gas response minus the brine response, called the ***hydrocarbon effect*** (right panel) is always −90° phase rotated with respect to the zero-phase wavelet.

To get a feel for the benefits of phase decomposition, we can look at the synthetic example of an intermediate impedance thin layer (with layer time thickness equal to a quarter of the dominant wavelet period) as shown in Figure 5a. The layer itself has a channel with reduced impedance relative to the inter-channel facies. The modeled synthetic response is shown in Figure 5b and the −90° phase component response is shown in Figure 5c. The wavelet used for generating the seismic response is a zero-phase Ricker wavelet, and the modeled response is displayed with SEG polarity, i.e., a positive reflection coefficient is represented as a peak. This polarity convention is used for all displays shown in this article.

The slight changes in amplitude caused by the channel change the reflection coefficients slightly, but the lateral variation in the amplitude caused by the channel is small enough and may not be recognized on conventional seismic data. This implies that any amplitude or phase anomaly that we may expect due to the channel will be weak and may not be detected on the seismic traces. However, the channel is revealed as highly anomalous on the −90° phase component.

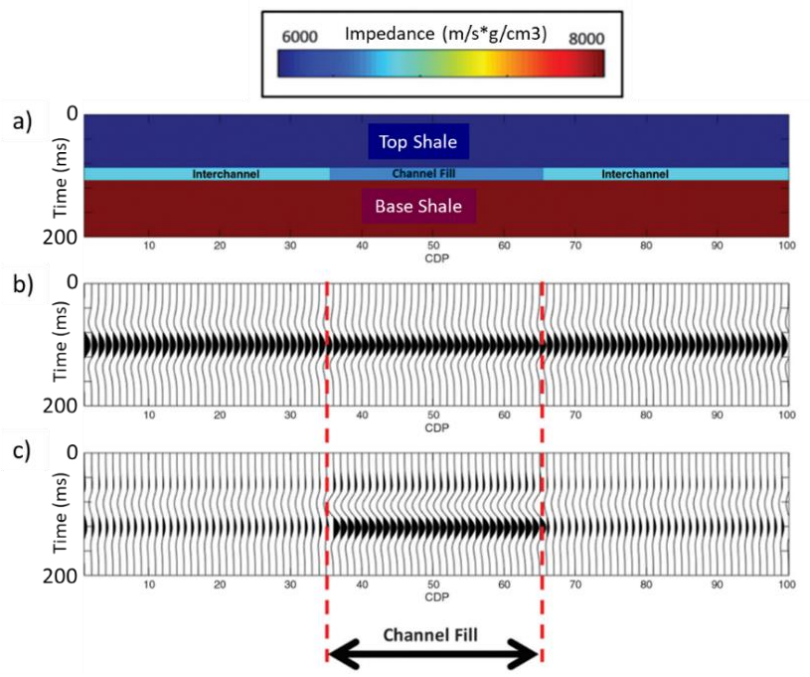

Figure 5: (a) A hypothetical geological model showing a change in impedance in the thin layer containing a channel. (b) Modeled synthetic amplitude response does not show the amplitude anomaly corresponding to the thin impedance layer, and (c) the computed −90° phase component exhibits a strong amplitude anomaly for the thin impedance channel. (Castagna et al., 2016)

Likewise, phase decomposition can be used as a reconnaissance tool when hydrocarbon anomalies associated with a range of thicknesses are expected to be seen on seismic data. The resolved reflections on the different phase components may not show any difference from the zero-phase input seismic data, but the bright spots associated with thin low-impedance reservoirs may exhibit a strong anomaly on the −90° phase component.

Besides generating the complete phase gathers for the input data, it is also possible to generate the individual phase components, and it is found that the ones at 0°, 180°, −90° and +90° appear to be very useful. As has been mentioned earlier, for zero-phase seismic data the computed −90° phase component can exhibit a strong amplitude anomaly for the thin low-impedance channel sands. However, impedance changes within the individual layers in the zone of interest can cause the top reflection coefficient to become slightly more negative, and the lower one to become more positive. Such asymmetry in reflection coefficients can show up better on the ±90° components. It therefore helps to compute the sum of +90° and −90° phase components, which we refer as the odd component, and the sum of the 0 and 180° phase components, referred to as the even component. A comparison of the odd and the even components, or the odd component with the input seismic data, can help in the direct detection of hydrocarbon zones, as the following applications will illustrate.

Application of phase decomposition analysis on real data and its comparison with results from a detailed impedance inversion workflow

For illustrating the importance of phase decomposition analysis, a stacked seismic volume from Denmark shot over a natural gas storage structure is considered here as shown in Figure 6. Natural gas storage serves as a good buffer in the supply and demand cycles and ensures reliable and responsive delivery of natural gas during times of peak demand. Such a storage is usually carried out in depleted oil and gas reservoirs, aquifers, and salt cavern formations, which are close to consumption sites. In other cases, natural aquifers have been converted to natural gas storage reservoirs. Besides the physical characteristics (porosity, permeability, capacity, and retention capability) of a reservoir, the deliverability rate and injection rate are other considerations for natural gas storage reservoirs.

In Denmark, there are two underground gas storage facilities that serve as a buffer for supply of gas from the North Sea. The first one is the salt caverns in Jylland, and the other is a deep aquifer at a depth of 1500 m near Stenlille, located approximately 30 km southeast of the Havnsø CO_2 storage prospect.

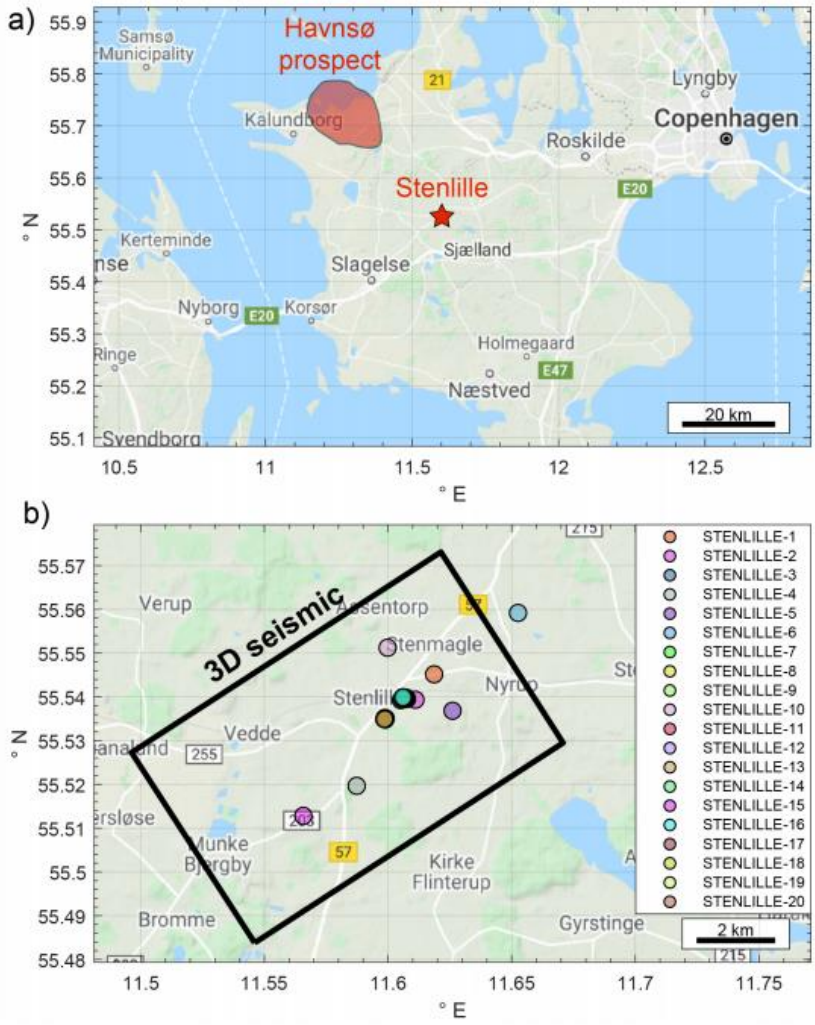

Figure 6: Location maps of (a) Sjælland with the Havnsø prospect outlined, and (b) zoom in at the Stenlille area showing location of 20 wells and the limits of the 3D seismic survey. Many wells have approximately the same position and plot on top of each other on the map. Courtesy of Google Maps. (After Bredesen, 2022)

Natural gas has been injected and stored at Stenlille since 1989, where the reservoir occurs within a domal subsurface structure and is covered by the tight Fjerritslev Formation caprock (Figure 7). The Upper Triassic Gassum Formation forms the natural gas storage reservoir and consists of interbedded sandstones and mudstones. Overlying the Gassum Formation is the 300 m thick Lower Jurassic sandstone Fjerritslev Formation, which consists of marine mudstones and shales, and is the regional caprock. The storage capacity of the Stenlille structure has been estimated to be three billion cubic meters, but due to reservoir heterogeneity, the gas is stored in several separate zones. Below the Gassum Formation are the impermeable mudstones of the Vinding, Oddesund, and other older formations, notably the Zechstein Formation at approximately 2800 m below the surface, where the salt movements resulted in the formation of the Stenlille structure.

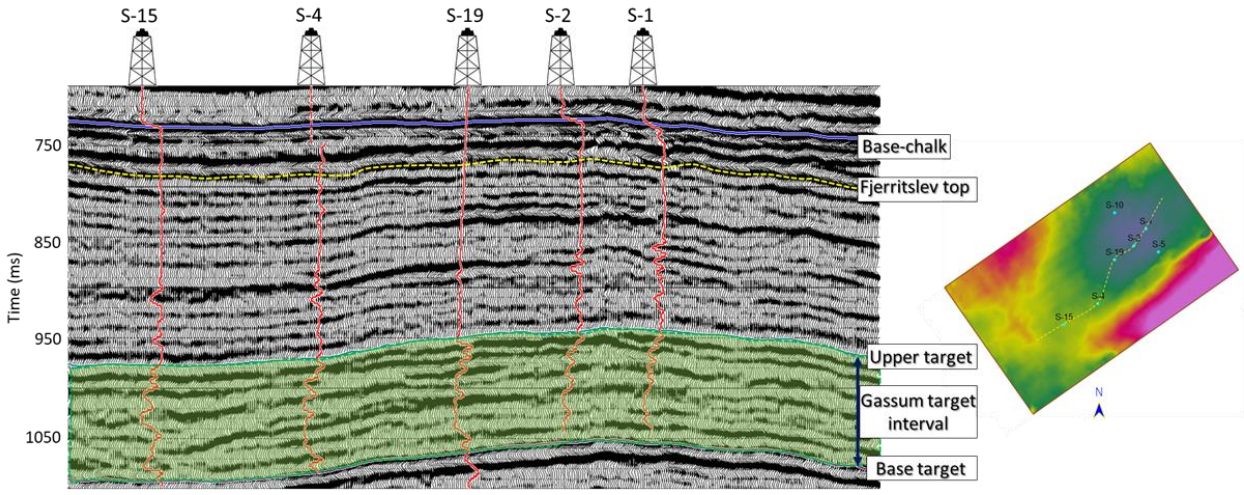

Figure 7: Correlation of gamma-ray logs with seismic data along an arbitrary line passing through the available wells as shown on the base map alongside. The shaded green area represents the zone of interest.

At the Stenlille facility, the natural gas is stored in an anticline structure defined by six sandstone reservoir zones in the Gassum Formation. The Gassum sandstone reservoir is approximately 140 m thick, but only the upper 40 m is used for storage in order to prevent gas migration through the spill-point. The upper 40 m are divided into five gas storage zones segregated by thin shale beds (Figure 8) which operate as two separated units, namely zones 1-3 operating as one integrated unit, and zone 5 which is located below. The estimated total gas storage volume is 3 billion cubic meters within the four-way closure, covering an area of approximately 14 km^2.

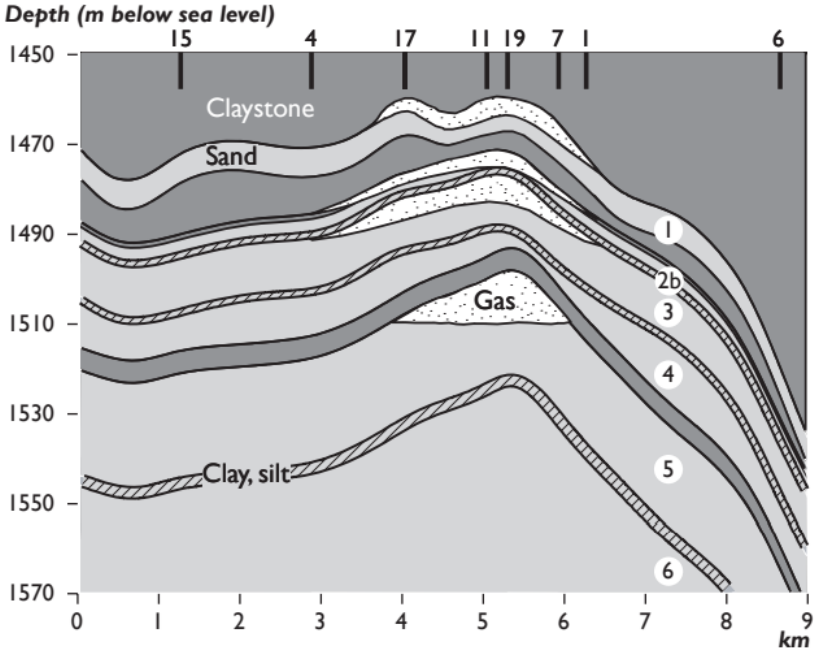

Figure 8: Schematic cross section (SW–NE) of the Stenlille natural gas underground storage showing the various reservoir zones. Well locations are indicated at the top of the figure. (Adapted from Laier and Øbro, 2009).

To get a greater insight into the phase decomposition process, the well curves for a deep well (S-19) in the natural gas storage reservoir area described above were picked up. We show some of the available curves in Figure 9, where left-to-right, the porosity and fluid saturations, shale volume, acoustic impedance, and the V_P/V_S logs are seen covering the broad reservoir zone. The upper part of the target zone is characterized by more interchanging shale and sand beds (zone 1-4), whereas zones 5 and 6 are composed of thicker units of clean sandstones with an average porosity of approximately 27%. An 11 m gas column with approximately 70% gas saturation is located in the top of zone 5 sandstone (unit z5 ss in Figure 9). A 5-15 % gas saturation in the sandstone zones above are observed as well, as measured in 2001.

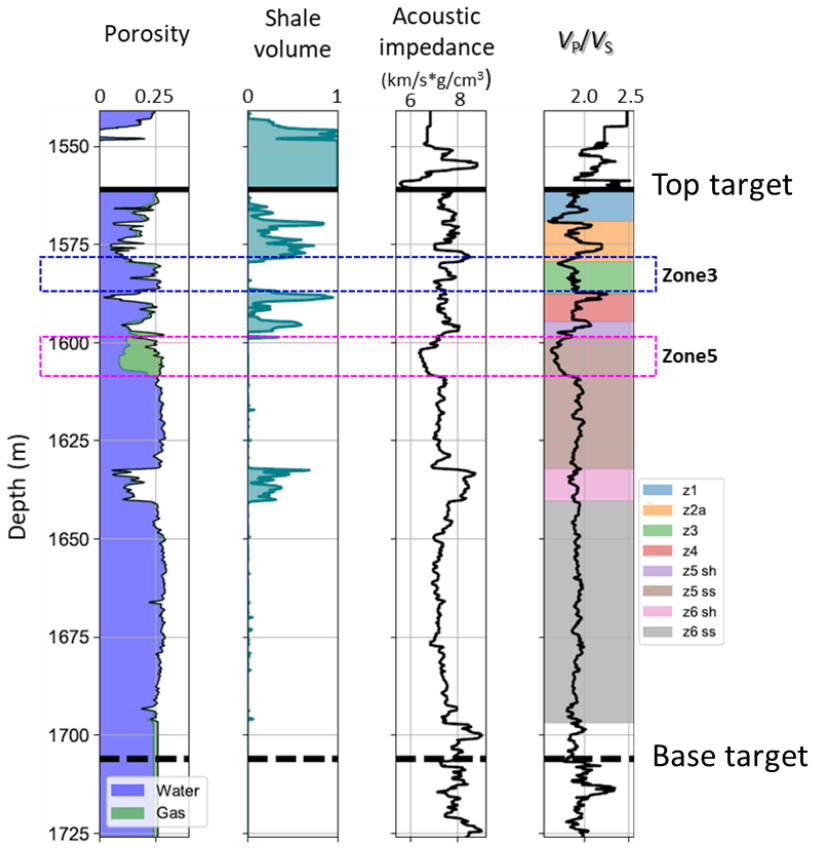

Figure 9: Well curves from Stenlille-19, from left-to-right: porosity, shale volume, acoustic impedance, and the P-to-S velocity ratio with reservoir zonation as background color. *(After Bredesen, 2022)*

In Figure 10 we show the well curve segments (V_P, V_S, density, V_{shale} and S_w) that cover the broad interval encompassing zones 3 and 5 reservoirs from well S-19 as well as a modeled elastic gather with angles of incidence up to 45°. An amplitude increase with angle is seen at the level of zone 5 (green arrow), but not at the level of zone 3 for this well (exhibits high values of S_w). The high amplitude reflection on the synthetic gather indicated with the yellow block arrow seems to have been generated due to the velocity and density changes seen on the curves, but this reflection is outside the zone of our interest.

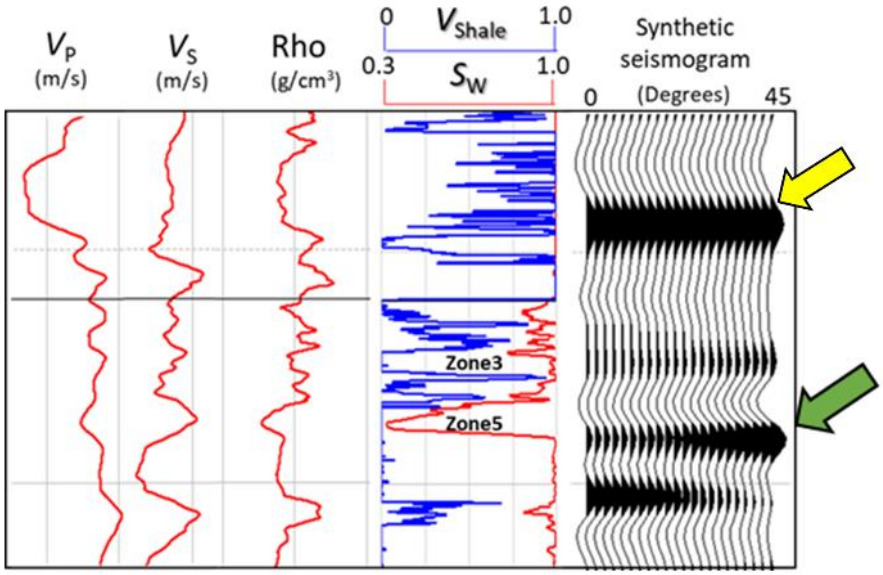

Figure 10: Well curve segments (V_P, V_S, density, V_{shale} and S_w) covering the broad interval encompassing zones 3 and 5 reservoirs for well S-19 as well as a modeled elastic gather. An amplitude anomaly corresponding to the gas is seen at the level of zone 5 (green arrow).

Next, fluid replacement modeling was carried out using the Gassmann fluid substitution (Gassmann, 1951), where the gas in zone 5 (green arrow) was first replaced with 100% brine to eliminate pore fluid effects. In Figure 11, the well curves with fluid replacement are shown in blue and overlaid on the input curves in red. The generated elastic gather equivalent to the one in Figure 10 does not show any amplitude anomaly. Similarly, when the brine in zone 3 (cyan arrow) is replaced with gas in the input well curves, the equivalent elastic gather (Figure 11b) shows amplitude anomalies at both levels.

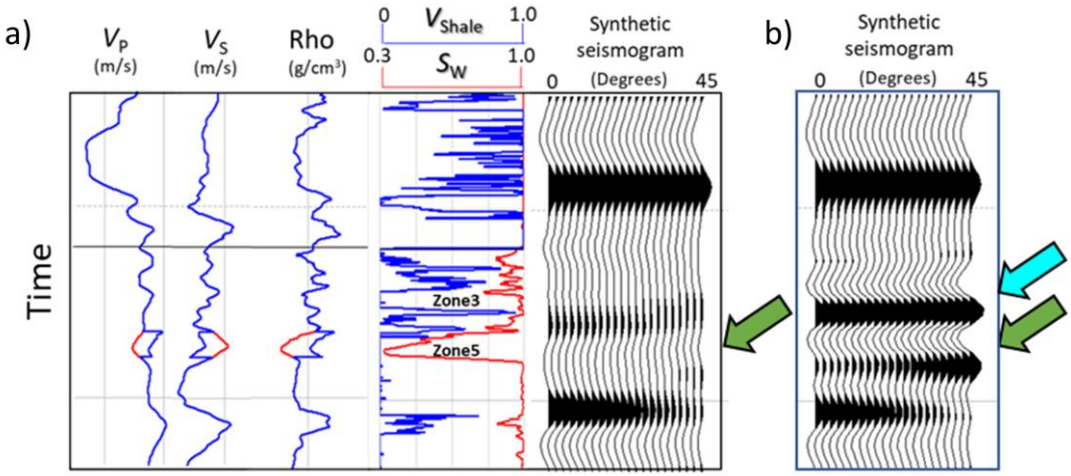

Figure 11: (a) Fluid replacement modeling carried out at the level of zone 5 (green arrow), where the natural gas was replaced with brine. As expected, no amplitude anomaly is now seen. (b) When the brine in zone 3 (cyan arrow) is replaced with gas and with gas already present in zone 5, amplitude anomalies are seen corresponding to both gas zones.

We take this exercise forward and generate phase gathers for each of the three cases discussed above, i.e., using the elastic gathers shown in Figure 10, 11a and 11b. The results are shown in Figure 12.

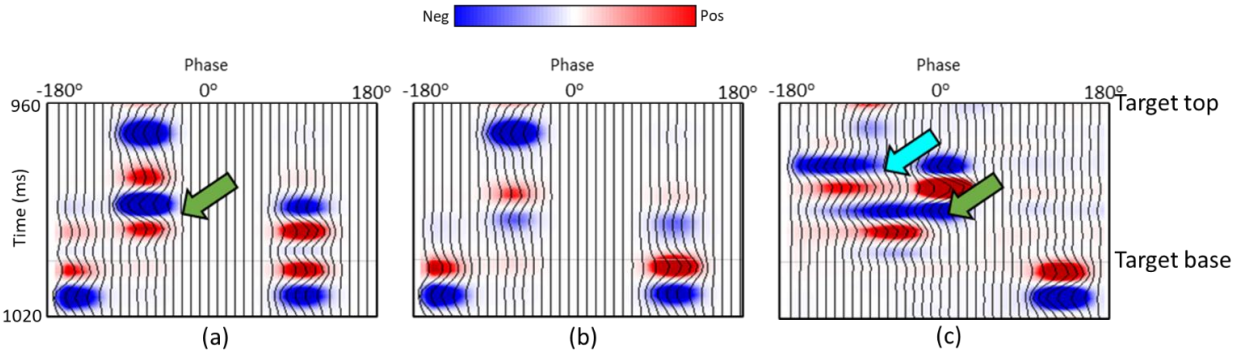

Figure 12: Phase gathers generated when (a) zone 3 is brine saturated and zone 5 is gas saturated, (b) both zone 3 (cyan arrow) and zone 5 (green arrow) are brine saturated, and (c) both zone 3 and zone 5 are gas saturated. As expected, no amplitude anomalies are seen for the brine saturated case but are seen whenever gas is present in the reservoir zone.

Finally, the odd phase components were generated for the synthetic gathers generated for each of the cases with fluid replacement modeling and the equivalent real seismic gather. Their comparison is shown in Figure 13. We notice that an amplitude anomaly is seen on the odd phase component when gas is present in a reservoir zone, which is an encouraging observation and can be used for mapping the spatial and temporal distribution of gas reservoirs.

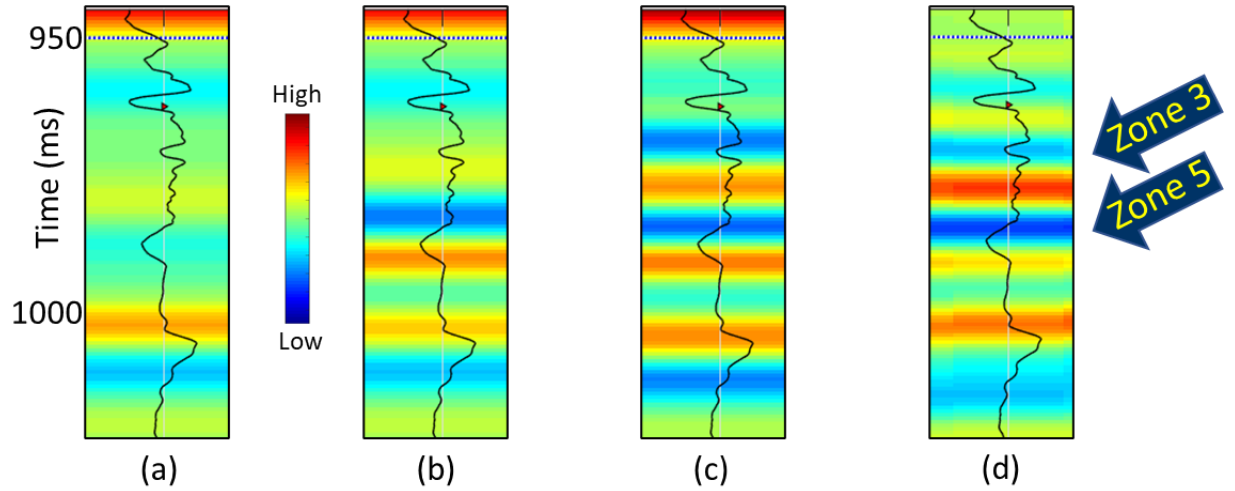

Figure 13: Comparison of odd phase components generated for synthetic phase gather for (a) both zone 3 and zone 5 as brine saturated, (b) zone 5 as gas saturated but zone 3 as brine saturated, and (c) both zone 3 and zone 5 as gas saturated. (d) Odd phase component generated for the real phase gather. An amplitude anomaly is expected on the odd phase component when gas is presented in a reservoir zone, which is evident on both synthetic and real data as indicated by the blue block arrows.

Armed with this interesting information we attempt to compare the results with the one obtained from a detailed approach entailing deterministic poststack impedance inversion along with neural network analysis to predict a porosity volume as well as understand the facies variation within the target zone (Bredesen, 2022). Probabilistic impedance/facies inversion was also carried out for predicting the gas probability volume. Discontinuity attributes such as multispectral coherence, multispectral curvature, and fault likelihood, were carried out on post-stack seismic data, for understanding the fault/fracture system to mitigate the gas leakage problem, and have been discussed by Bredesen (2022).

In Figure 14a we show a segment of an inline from the seismic data volume passing through well S-19. The equivalent sections from the odd phase component stacked data and the sandstone gas probability volume are shown in Figures 14b and c, respectively. While it is difficult to identify amplitude anomalies on input seismic data within the ZOI, a prominent amplitude anomaly corresponding to zones 3 and 5 is evident on the odd phase component section which correlates reasonably well with the high probability gas sandstone reservoir zones. Such a comparison lends confidence in phase decomposition analysis. However, the gas probability for zone 3 is seen as smeared laterally and will be seen on stratal displays shown in the next section.

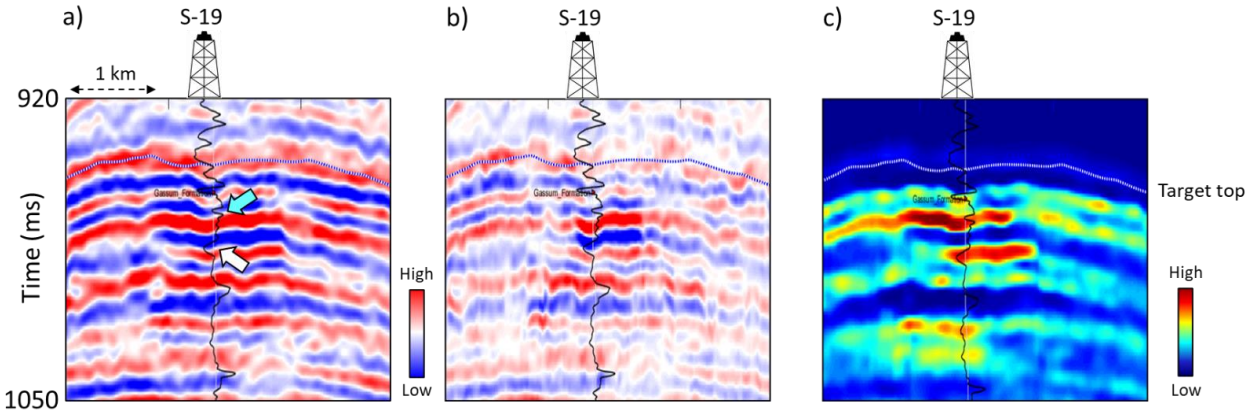

Figure 14: (a) An inline section from the PSTM stacked volume passing through well S-19. (b) Equivalent inline section from the odd phase (combination of −90° and +90° event phases) component volume. (c) Equivalent inline section from gas probability volume. The level of zone 3 reservoir is indicated with the cyan block arrow and that for reservoir zone 5 with a white arrow. Notice, the lateral spread of the zone 3 and 5 reservoirs clearly on the odd phase component (Figure 14b), but the sandstone gas probability display exhibits smeared anomaly for zone 3, which is not supported by seismic interpretation.

Attempts at reservoir characterization

Deterministic poststack impedance inversion as well as a neural network approach was used to predict the porosity volume as well as understand the facies variation within the target zone. Probabilistic impedance inversion was also carried out for predicting the gas probability volume (Bredesen, 2022).

Before considering the spatial comparison, it is important to discuss the available well-log data. There are 20 wells drilled over the Stenlille 3D area, of which fourteen are operational gas injection and withdrawal wells, and six are observation wells (ST-3, 4, 5, 6, 10, and 15) for monitoring pressure in the aquifer around the reservoir and in the caprock (Figure 6). Of the 14 operational wells for zone 1-3, wells ST-2, 7, 9, and 11 are the main injectors and ST-12 is the main producer, though in recent years ST-11 and ST-12 have been the main injection/withdrawal wells, respectively. All wells are designed as injection/withdrawal wells. Gas injection began in 1989 in zone 1-3 and was registered during the first few years of the gas storage establishment in the ST-4 observation well. Then from June 1995, gas was subsequently injected into zone 5.

In Figure 15a, the seismic stratal slice shows the gas anomaly for zone 1-3 in blue with the wells ST-11, 12, 07 and 17 touching it, implying they are associated with storage or retrieval of gas in the reservoir. Multispectral coherence (Chopra and Marfurt, 2018) has been overlaid in black, using transparency. The equivalent display in Figure 15b is from the odd phase (combination of −90° and +90° phase components) component volume, where the blue anomaly is seen as more compact, exhibiting less variation as compared with the other two displays. The faults marked with purple block arrows appear to be acting as fluid barriers, with the anomaly on the odd phase component following them closely. The gas anomaly towards the southwest is stronger in Figures 15b and 15c than in Figure 15a suggesting significant gas migration in that direction. The equivalent display shown in Figure 15c is from the gas probability volume that was generated using probabilistic impedance inversion using stacked input seismic data. We notice that the anomaly corresponding to gas probability is spread out and does not exhibit a more constrained fluid distribution as in the seismic odd phase component (Figure 15b). Notice that the odd phase map predicts less gas around ST-2 and in the area southeast of the most prominent fault lineament in the NE-SW direction. This is an interesting observation because the injection history from ST-2 in Figure 6a shows that approximately 130 m^3 of gas was injected into this well prior to the seismic survey. This well also seems to be isolated from the other wells on the southern side of the prominent fault barrier. The odd phase map still shows a blue anomaly close to ST-2, though much less outstanding than in the gas probability map. Thus, the odd phase component display allows more accurate interpretation.

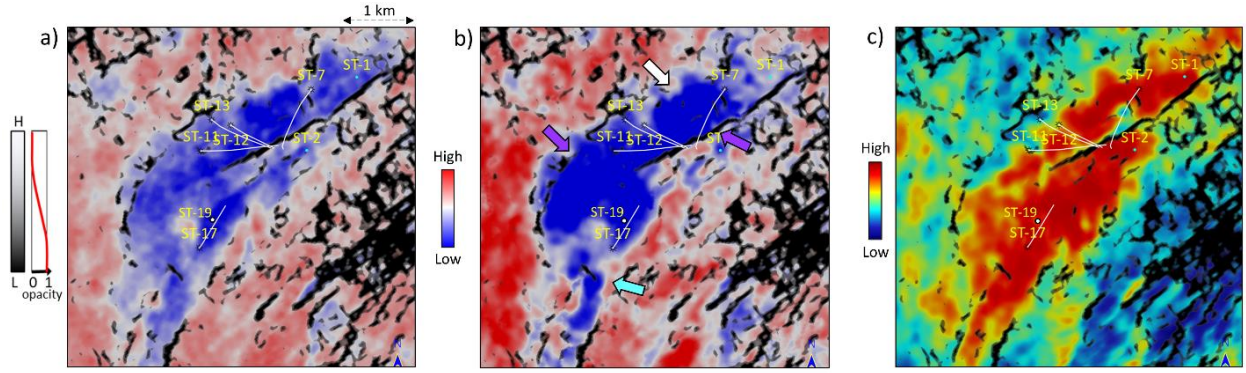

Figure 15: Stratal slices at the level of gas zone 1-3 from (a) input seismic data, (b) odd phase component stacked data, and the (c) gas sandstone probability volumes. The gas probability volume was generated using probabilistic impedance inversion (Bredesen, 2022). On each display multispectral coherence has been overlaid in black using transparency. The odd phase component display appears to be less patchy and laterally more continuous than the gas probability display. The horizontal wells are known to traverse continuous reservoir along their paths, which is more in accordance with the odd phase magnitude display.

The gas distribution from the odd phase map also appears to be more convincing with regards to the gas fluid movement towards northwest, where it nicely conforms with the multispectral coherence attribute and looks more like what may be suspected as the shape of a growing gas plume in a homogenous sandstone reservoir (a circle/ellipse shape rather than a fingering/channeling distribution that does not conform well with the northwest fault barrier). This is also seen more clearly in the zone 5 map in Figure 16, whereas the gas probability map predicts more of a fingering/channeling fluid distribution that conforms not so well with the northwest fault barrier.

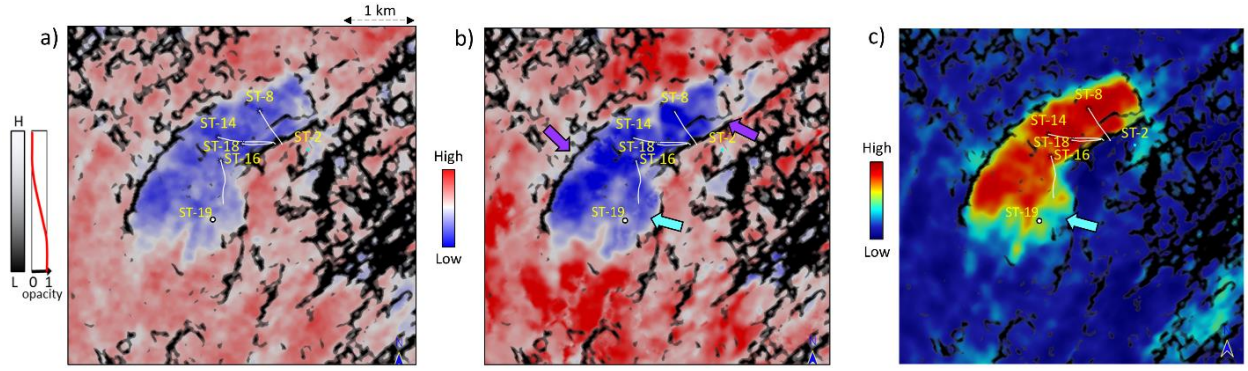

Figure 16: Stratal slices at the level of gas zone 5 from (a) input seismic data, (b) odd phase component stacked data, and the (c) gas sandstone probability volumes. The gas probability volume was generated using probabilistic impedance inversion (Bredesen, 2022). On each display multispectral coherence has been overlaid in black using transparency. The operational horizontal wells for zone 5 are also shown. The outline of the gas anomaly on the odd phase component display appears to be better defined than the seismic display as well as the variation in terms of the dark blue areas, and matches the higher gas probability prediction shown in Figure c. The display also shows much better correlation of the dark blue areas on the odd phase component with the wells.

It may be appropriately mentioned here that in a reservoir management context, small deviations in the spatial extent of a hydrocarbon anomaly as seen on different map displays could be valuable information in order to improve the understanding of fluid movement within the reservoir. Thus, what we surmise from these observations is that the odd phase component can provide detailed information, different from that seen on the input seismic amplitudes. A very good correlation of the horizontal wells operational for this zone is seen, with the toe of each well falling in the blue zone. Well S-19 is only slightly deviated and not be treated as a horizontal well.

The equivalent stratal slice comparison display at the level of zone 5 shown in Figure 16 again shows the gas anomaly to be better defined on the odd component (Figure 16b) display than the seismic amplitude display (Figure 16a). The gas probability display (Figure 16c) indicates the gas anomaly as well defined but is shrunk in size at the lower end as indicated by the light blue arrow. Again, the faults marked with purple block arrows on the multispectral coherence appear to be acting as fluid barriers, with the gas anomaly following them closely on all three displays. The gas anomaly also shows much better correlation of the dark blue areas on the odd phase component with the wells.

In Figure 17 we show a relative comparison of arbitrary sections traversing through wells S-04, S-17, S-18, S-02, and S-05, bounded by two horizons defining the target top and base, and extracted from the input seismic (Figure 17a), and the odd component (Figure 17b) volumes. The overlaid curve is the P-impedance log. Notice, in Figure 17a the seismic reflections are seen extending laterally over both wells S-17 and S-18 as well as above and below zones 3 and 5 of the reservoir as indicated with the yellow block arrows. It is difficult to assess the areal extent of zone 3 for well S-17 and for zone 5 for well S-18 on the input seismic display in Figure 17a. On examination of the equivalent section from the odd phase component, notice, the zone 3 gas anomaly correlates well with the impedance log and looks clearly defined both laterally and vertically for well S-17. Similarly zones 3 and 5 for well S-18 clearly correlate with the impedance log. The faults on both sides of the reservoir are also seen well-defined and are thus marked clearly with green dashed lines. These faults are also seen bounding zone 3 and zone 5 gas accumulations in Figures 15 and 16. Wells S-04 and S-05 are observation wells. S-02 is an injector well associated with storage and retrieval and could exhibit some gas signature. As a result, a feeble gas signature is seen for well S-02 as expected.

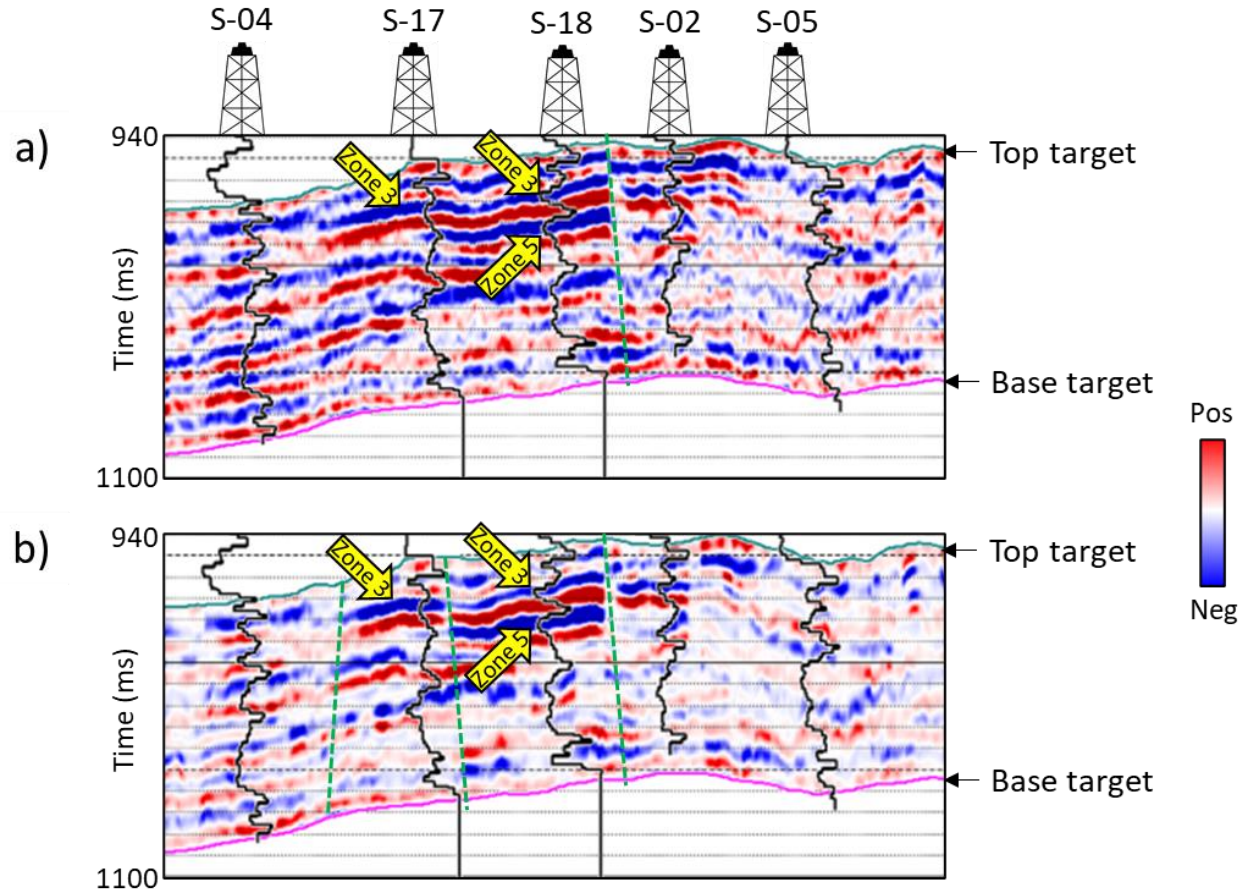

Figure 17: An arbitrary line passing through wells S-04, S-17, S-18, S-02, and S-05 and extracted out of the (a) seismic, and (b) odd component volumes. P-impedance logs are overlaid on the two displays. Well S-18 has gas in both zones 3 and 5, and well S-17 has gas in zones 3 only. Wells S-04 and S-05 are observation wells, S-02 is an injector well associated with storage and retrieval and could exhibit some gas signature. Notice, it is difficult to distinguish zones 3 and 5 for wells S-17 and S-18 on the seismic display but they are clearly distinguished on the odd component display (Figure 17b) separated by almost vertical faults. Their signature correlation with the impedance logs is seen to be quite good. A feeble gas signature is seen for well S-02 as expected.

Discussion

In many regions around the world production is expected from thin sandstone or carbonate reservoirs. Because the seismic waves are bandlimited with low-frequency content, a thin reservoir implies that the thickness of the reservoir is at or less than a quarter wavelength of the seismic waves (following Widess's (1973) criterion). Thus, if the average spectrum of a seismic wavelet is centered around 30 Hz, which is usually the case, reservoirs having a thickness less than 25 m, may not have their top and base reflectors resolved. This may suffice for structural objectives, but stratigraphic targets are usually set to look for reservoirs 10 m or less in thickness. In such thin reservoirs the reflection response would comprise interference of reflections from the top and the base of the thin layers. Exercises aimed at characterizing thin

reservoirs frequently neglect such interference effects, resulting in inaccurate reservoir characterization.

The phase decomposition discussed above finds useful applications subject to some caveats including that the seismic data being considered have a zero-phase embedded wavelet, the thicknesses of the zones of interest are at or below tuning at the CWT frequency used, and the seismic response has an absence of interference from adjoining reflectors. The application of phase decomposition to data that does not have one or more of the above conditions satisfied may not yield optimum results.

The first question that pops up then is, what happens when the embedded wavelet in the seismic data is different from zero-phase? If the input seismic data are not zero-phase, then attempts could be made to get the data reprocessed to zero phase for a meaningful application of phase decomposition. Not only that, zero-phase data will help with more accurate interpretation. If that is not possible for some reason, i.e., if the seismic wavelet is not zero phase, the phase component where specific responses are expected, should be modified accordingly. For example, if a −90° signal is expected with a zero-phase wavelet, that response would be found on the -60° component if the wavelet phase were 30°.

If the layer of interest is above seismic tuning, low-pass filtering (for example by stacking low CWT frequencies) can be used to lower the frequency content and push the layer of interest below tuning. This is called ***seismic thinning***, and its applications for distinguishing target anomalies have been discussed by Meza et al. (2016) and Barbato et al. (2017).

Attempts should be made to alleviate such problems and could include wavelet shaping of the embedded wavelet if it is not zero phase, using CWT spectral decomposition with a Ricker wavelet at higher frequency (but not high enough to go above tuning), and finally the phase decomposition analysis could be carried out on the required phase as read off from the phase gather, or what may be referred to as phase filtering. Though not discussed here, some of these issues will be discussed in future articles.

Conclusion

Phase decomposition can be used as a tool for direct interpretation of data in terms of impedance variations as well as a reconnaissance tool. For doing these interpretations, not only the phase gathers but the individual phase components can also be generated, the ones at 0°, 180°, −90° and +90° appearing to be most useful. The first two phase components can be combined into an even component volume, and the latter two into an odd component volume. Thin-bed seismic anomalies associated with hydrocarbons can be conveniently analyzed by interpreting these two data volumes. We have also introduced the application of phase decomposition as a reservoir management tool, with the odd phase component (sum of +90°

and −90° phase components) showing better correlation with the wells that control the injection and withdrawal of natural gas in the Stenlille reservoir zones. Based on the comparison of odd phase component and sandstone gas probability, the delineation of the gas reservoir zone on the odd component displays correlates better with the status of the available well data.

The present application of odd phase component has been attempted on legacy data, but if the legacy data are reprocessed to take advantage of the modern reprocessing techniques and their value-addition, it is anticipated that more accurate results will be forthcoming.

Acknowledgements

The first author would also like to thank the Geomodeling Technology Corporation for making the Attribute Studio software available, which has been used for some visualization displays shown in this paper, as well as the Attribute-Assisted Seismic Processing and Interpretation (AASPI) Consortium, University of Oklahoma, for access to their software, which has been used for all attribute computation.

References

Barbato, U., O. Portniaguine, B. Winkelman and J. P. Castagna, 2017, Phase decomposition as a DHI in bright spot regimes: A Gulf of Mexico case study, *87th Annual International Meeting, SEG, Expanded Abstracts*, 3976–3980. https://doi.org/10.1190/segam2017-17737608.1

Bredesen, K., 2022, Assessing rock physics and seismic characteristics of the Gassum Formation in the Stenlille aquifer gas storage – A reservoir analog for the Havnsø CO_2 storage prospect, Denmark, *Int. J. of Greenhouse Gas Control, 114, [103583]*.

Castagna, J., Sun, S. and Siegfried, R., 2003, Instantaneous spectral analysis: Detection of low-frequency shadows associated with hydrocarbons. *The Leading Edge*, **22**(2), 120 – 127. https://doi.org/10.1190/1.1559038

Castagna, J. P., A. Oyem, O. Portniaguine, and U. Aikulola, 2016, Phase decomposition, *Interpretation*, **4**(3), SN1–SN10. https://doi.org/10.1190/INT-2015-0150.1

Chakraborty, A., and D. Okaya, 1995, Frequency-time decomposition of seismic data using wavelet-based methods, *Geophysics*, **60**(6), 1906–1916. https://doi.org/10.1190/1.1443922

Chopra, S., and K. J. Marfurt, 2018, Multispectral, multiazimuth and multioffset coherence attribute applications, *Interpretation*, **7**(2), SC21-SC32. https://doi.org/10.1190/INT-2018-0090.1

Laier, T., and H. Obro, 2009, Environmental and safety monitoring of the natural gas underground storage at Stenlille, Denmark, in Underground gas storage: worldwide experiences and future development in the UK and Europe, Eds. D.J. Evans, R.A. Chadwick, Geol. Soc. London, 81-92.

Lindner, R. R., C. Vera-Ciro, C. E. Murray, S. Stanimirovic, B. Babler, C. Heiles, P. Hennebelle, W. M. Goss, and J. Dickey, 2015, Autonomous Gaussian Decomposition, *The Astronomical Journal*, **148**(4) 1-14. https://doi.org/10.1088/0004-6256/149/4/138

Mallat, S., and Z. Zhang, 1993, Matching pursuits with time-frequency dictionaries, *IEEE Transactions on Signal Processing,* **41**(12),3397–3415. https://doi.org/10.1109/78.258082

Meza, R., G. Haughey, J. P. Castagna, U. Barbato, and O. Portniaguine, 2016, Phase decomposition as a hydrocarbon indicator, A case study: *86th Annual International Meeting, SEG, Expanded Abstracts*, 1839–1943. https://doi.org/10.1190/segam2016-13871199.1

Partyka, G., Gridley, J., and Lopez, J. [1999] Interpretational applications of spectral decomposition in reservoir characterization, *The Leading Edge*, **18**(3), 353 – 360. https://doi.org/10.1190/1.1438295

Portniaguine, O. and J. P. Castagna, 2004, Inverse spectral decomposition, *74th Annual International Meeting, SEG, Expanded Abstracts*, 1786-1789. https://doi.org/10.1190/1.1845172

Portniaguine, O. and J. P. Castagna, 2005, Spectral inversion: Lessons from modeling and Boonesville case study, *75th Annual International Meeting, SEG, Expanded Abstracts*, 1638-1641. https://doi.org/10.1190/1.2148009

Puryear, C. I., O. Portniaguine, and C. Cobos, J. P. Castagna, 2012, Constrained least-squares spectral analysis: Applications to seismic data, *Geophysics*, **77**(5), ISO-Z132. https://doi.org/10.1190/geo2011-0210.1

Sinha, S., P. S. Routh, P. D. Anno, and J. P. Castagna, 2005, Spectral decomposition of seismic data with continuous-wavelet transforms, *Geophysics*, **70**(6), 19–25. https://doi.org/10.1190/1.2127113

Stockwell, R., L. Mansinha, and R. Lowe, 1996, Localization of the complex spectrum: the s transform, *IEEE Transactions on Signal Processing*, **44**(4), 998–1001. https://doi.org/10.1109/78.492555

Widess, M. B., 1973, How thin is a thin bed? Geophysics, **38**(6), 1176-1180. https://doi.org/10.1190/1.1440403

About the Authors

Satinder Chopra *is the founder and President of SamiGeo Consulting Ltd., based in Calgary. He has 37 years of experience as a geophysicist specializing in processing, special processing, interactive interpretation of seismic data and reservoir characterization. His research interests focus on techniques aimed at characterization of reservoirs. He has published eight books and more than 500 papers and abstracts. His work and presentations have won several awards from international professional societies the most notable ones being the 2021 Roy O. Lindseth CSEG Medal Award (2021), AAPG Distinguished Service Award (2019), EAGE Honorary Membership (2017), CSEG Honorary Membership (2014), Meritorious Service (2005) Award, 2014 APEGA Frank Spragins Award, the 2010 AAPG George Matson Award, and the 2013 AAPG Jules Braunstein Award. He has been the 2010/11 CSEG Distinguished Lecturer, the 2011/12 AAPG/SEG Distinguished Lecturer, and the 2014/15 EAGE e-Distinguished Lecturer.*

Ritesh Kumar Sharma *is with Calgary-based SamiGeo. He has vast experience of working with 2-D/3-D, land, and marine seismic data with different applications such as AVO analysis, rock-physics analysis, frequency enhancement of seismic data, simultaneous inversion, extended elastic impedance inversion as well as geostatistical inversion. He is an active member of SEG and CSEG.*

John Castagna *holds the Sheriff Chair in Geophysics at the University of Houston. His main research interest is the quantitative interpretation of seismic data.*

Kenneth Bredesen *works as a geophysicist at the Geological Survey of Denmark and Greenland (GEUS). He received a Ph.D. in geophysics from the University of Bergen in 2017. He has previously worked as a QI geophysicist at Spike Exploration and as a postdoctoral researcher at Aarhus University. His core competencies are quantitative seismic interpretation, rock physics modeling, seismic attributes, and amplitude analysis.*